Received: 24 September 2024 | Revised: 28 November 2025 | Accepted: 23 December 2025

DOI: 10.1002/qj.70114

Quarterly Journal of the Royal Meteorological Society RMetS

RESEARCH ARTICLE

Using a causal effect network approach to quantify the impact of ENSO teleconnections on summer monsoon precipitation over the Himalayas and key regional circulations

Grzegorz Muszynski[1,2] | **Andrew Orr**[1] | **Indrani Roy**[3] | **Giorgia Di Capua**[4,5] | **Hamish D. Pritchard**[1] | **J. Scott Hosking**[1,6]

[1]British Antarctic Survey, Natural Environment Research Council, Cambridge, UK

[2]Atmospheric, Oceanic and Planetary Physics (AOPP), Department of Physics, University of Oxford, Oxford, UK

[3]Department of Earth Sciences, University College London, London, UK

[4]Department of Water, Environment, Construction and Safety, Magdeburg–Stendal University of Applied Sciences, Magdeburg, Germany

[5]Department of Earth System Analysis, Potsdam Institute for Climate Impact Research, Potsdam, Germany

[6]The Alan Turing Institute, London, UK

Correspondence
Grzegorz Muszynski, AOPP, Department of Physics, University of Oxford, Oxford, UK.
Email: muszynski.grzegorz.tda@gmail.com

Funding information
UKRI Strategic Priorities Fund under the EPSRC, Grant/Award Numbers: EP/T001569/1, EP/W006022/1; UKRI/NERC, Grant/Award Number: NE/X005267/1; JPI Climate/JPI Oceans NextG-Climate Science ROADMAP, Grant/Award Number: 01LP2002B; HORIZON-RIA project, Grant/Award Number: 101081276

Abstract

We perform a causal analysis to quantify the direct causal links on intraseasonal time-scales associated with the influence of El Niño–Southern Oscillation (ENSO) teleconnections on summer monsoon Himalayan precipitation (SMHP) and two key coupled regional circulations, which are the monsoon Hadley circulation (MHC) and the component of the regional Walker circulation (RWC) over the Himalayas. This is achieved by using a causal effect network (CEN) approach to show graphically the direction and strength of linkages between four monthly climate indices representing ENSO, SMHP, RWC, and MHC from 1940 to 2022 with a time lag of one month. Depending on the complexity of the CENs constructed, the results show causal effect (CE) values as follows: (i) ENSO to SMHP of −0.33 to −0.44 (i.e., a one standard deviation increase in ENSO causes a decrease in SMHP of between −0.33 and −0.44 standard deviations with a lag of one month), (ii) ENSO to MHC of −0.12 to −0.15, and (iii) ENSO to RWC of −0.17 to −0.20. These are interpreted as an increase in ENSO (analogous to the El Niño phase) causing a substantial decrease in Himalayan precipitation, as well as weakening the key regional circulations. Further results showed CE values from MHC to SMHP of 0.32 to 0.43 and from RWC to SMHP of 0.30 to 0.37. These are interpreted as a strengthening of both the regional Walker circulation and the monsoon Hadley circulation causing a substantial increase in Himalayan precipitation. Finally, the approach was used to clarify the coupled interactions between RWC and MHC, which showed a CE value of 0.14 to 0.17 from RWC to MHC and from MHC to RWC. This suggests positive feedback between the two regional circulations.

KEYWORDS

causal effect networks, ENSO teleconnections, Himalayas, monsoon Hadley circulation, regional Walker circulation, summer monsoon precipitation

1 | INTRODUCTION

The Himalayas are the source of many major river systems in South Asia, with the largest being the Ganges, Indus, and Brahmaputra (Immerzeel *et al.*, 2010; Lutz *et al.*, 2014). These river systems provide crucial drinking water, irrigation supplies, and hydropower generation for hundreds of millions of people, as well as supporting numerous biodiverse-rich ecosystems (Mukherji *et al.*, 2019; Orr *et al.*, 2022; Wester *et al.*, 2019). A crucial contribution to these river systems is from the large amount of precipitation falling over the Himalayas due to the Indian summer monsoon (ISM) from June to September (Bookhagen & Burbank, 2010; Lutz *et al.*, 2014; Palazzi *et al.*, 2013, 2015). The ISM is closely associated with a regional monsoon Hadley circulation (MHC), which is a meridional overturning atmospheric circulation driven by intense solar heating over the Indian subcontinent and Tibetan Plateau during this period, with the high-altitude Tibetan Plateau ensuring that the heating occurs aloft (Choudhury & Krishnan, 2011; Gill, 1980; Li & Yanai, 1996; Rao, 1976; Yanai & Wu, 2006). The MHC is characterised by ascending motion over the heat source regions and descending motion around the Equator, as well as southerlies in the lower troposphere and northerlies in the upper troposphere. The Earth's Coriolis force causes the southerly winds to deflect to the right relative to their direction of travel, resulting in the formation of a low-level westerly jet across the Arabian Sea (Findlater, 1970; Turner & Annamalai, 2012), which is associated with enhanced moisture transport to the Indian subcontinent. The enhanced monsoonal winds/moisture transport eventually reach the Himalayas, which act as a large orographic barrier that contributes to the enhancement of the monsoon precipitation over this region (Bookhagen & Burbank, 2010; Galewsky, 2009; Orr *et al.*, 2017; Palazzi *et al.*, 2013, 2015).

Intraseasonal variability in ISM precipitation (i.e., variations occurring within a monsoon season) is known to be strongly influenced by changes in sea-surface temperatures over the tropical Pacific Ocean associated with El Niño–Southern Oscillation (ENSO), with El Niño the warm phase of the teleconnection and La Niña the cold phase. El Niño events are usually associated with below-average ISM precipitation and La Niña events with above-average ISM precipitation (Gill *et al.*, 2015; Krishnamurthy & Goswami, 2000; Kumar *et al.*, 1999; Mishra *et al.*, 2012; Mukherjee *et al.*, 2020; Rasmusson & Carpenter, 1983; Roy *et al.*, 2017; Turner *et al.*, 2005; Wang *et al.*, 2012; Webster & Yang, 1992). ENSO causes large variability in the planetary-scale Walker circulation, which consists of multiple zonal atmospheric overturning cells in the Tropics, including a Pacific Ocean Walker circulation and an Indian Ocean Walker circulation that influence the ISM (Goswami, 1994, 1998; Gushchina *et al.*, 2020; Kumar *et al.*, 1999, 2006; Nigam, 1994; Sikka, 1980; Webster & Yang, 1992). During ENSO neutral conditions, the Pacific component is characterised by ascending motion over the relatively warm waters of the western Pacific and descending motion over the relatively cool waters of the eastern Pacific (Bjerknes, 1969; Lau & Yang, 2003), while the Indian Ocean component is characterised by ascending motion over the eastern Indian Ocean and descending motion over the western Indian Ocean, as well as westerlies in the lower troposphere and easterlies in the upper troposphere (Cai *et al.*, 2013; Kohyama *et al.*, 2021). By contrast, the El Niño phase of ENSO is associated with anomalous warm waters over the eastern tropical Pacific, accompanied by increased convection over this region. This results in ascending motion over this region and descending motion over the western Pacific, that is, a reversal of the Pacific Ocean Walker circulation. Since this downward branch is also close to the eastern Indian Ocean, it also results in a weakening of the upward branch of the Indian Ocean Walker circulation. This therefore results in a weakening of the westerly wind component of the Indian Ocean Walker circulation, and therefore also a weakening of the low-level westerly jet across the Arabian Sea associated with the MHC, resulting in reduced ISM precipitation (Goswami, 1994, 1998; Gushchina *et al.*, 2020; Kumar *et al.*, 2006; Nigam, 1994; Sikka, 1980; Webster & Yang, 1992). Furthermore, the La Niña phase of ENSO is usually associated with anomalous warm waters occurring over the western tropical Pacific, which is accompanied by increased convection over this region. This results in a strengthening of the upward branch of the Pacific Ocean Walker circulation and therefore a strengthening of the upward branch of the Indian Ocean Walker circulation. This therefore causes a strengthening of the westerly wind component of the Indian Ocean Walker circulation, and therefore also a strengthening of the low-level westerly jet across the Arabian Sea associated with the MHC, resulting in enhanced ISM precipitation (Goswami, 1994, 1998; Gushchina *et al.*, 2020; Kumar *et al.*, 2006; Nigam, 1994; Sikka, 1980; Webster & Yang, 1992).

Webster *et al.* (1998) were the first to show that the causal interactions between ISM precipitation, ENSO teleconnections, and circulation fields can be formalised in terms of three hierarchies of complexity, and provided causal graphs/diagrams describing them. The first form describes a simple system, where the variability in ISM precipitation is affected only by changes to ENSO. The second form describes a more complex system, where the relationship between ISM precipitation and ENSO can be complicated by interactions with other climate factors (e.g., the Walker and Hadley circulations), which may also include feedbacks. The last and most complex

form describes a tangled system, where each component of the system can interact with the others, and is also chaotic and unstable, making disentangling these interactions extremely difficult. Nevertheless, the relationship between the MHC and Walker circulation in different phases of ENSO, and how this is coupled to the variability of ISM precipitation, is still a relatively underexplored topic (e.g., Webster & Yang, 1992; Goswami, 1994; Kumar *et al.*, 1999; Roy, 2018). Moreover, studies examining the relationships between ENSO, circulation fields, and ISM mostly focus on all-India rainfall based on precipitation over the Indian subcontinent (e.g., Krishnamurthy & Goswami, 2000) and typically neglect investigation of the influence on Himalayan precipitation. Furthermore, Roy and Tedeschi (2016) and Roy *et al.* (2017) showed that the influence of ENSO on ISM precipitation over the Himalayas can be viewed as a superposition and/or interaction between the MHC and the component of the Walker circulation over the Himalayan region, which they referred to as a regional Walker circulation (RWC). This is consistent with the work of Goswami (1994), who considered this region as a merging point of these circulations, that is, both systems are similar to the second/-complex form described by Webster *et al.* (1998). Finally, the large orographic precipitation enhancement associated with the Himalayas makes its hydrological regime distinct from that of the Indian subcontinent (Bookhagen & Burbank, 2010; Palazzi *et al.*, 2013, 2015).

Previous studies on the influence of ENSO on ISM precipitation have been based almost solely on lagged correlation, linear regression, and other basic statistical measures (e.g., Mishra *et al.*, 2012; Bhatla *et al.*, 2016; Yang & Huang, 2021). However, correlation-based metrics do not necessarily detect cause–effect relationships, and hence their interpretability is limited. For example, two climate processes that are not influencing each other directly (i.e., not causally related) may show a high statistical correlation due to strong autocorrelation (e.g., if one of the processes depends on past values) and/or the effects of a common driver/third underlying factor (McGraw & Barnes, 2018; Runge *et al.*, 2014). These deficiencies around correlation-based approaches can be overcome by causal-discovery approaches such as the Peter and Clark momentary conditional independence (PCMCI) algorithm, which identifies the causal relationships between time series or climate indices (Runge, 2018; Runge *et al.*, 2014; Runge *et al.*, 2019). This method disentangles true causal links among the time series from spurious links that can occur when common drivers, indirect links, or strong autocorrelation are present. The causal links identified using the PCMCI algorithm can be represented graphically using a causal effect network (CEN), which shows both the direction and the strength of the links. This approach has been used previously to gain insights into various physical relationships of the climate system (Runge *et al.*, 2015, 2019). For example, CENs have been successfully applied to quantify the causal relationships involving stratospheric polar vortex variability (Kretschmer *et al.*, 2016, 2017), teleconnection pathways between the tropical and midlatitude regions (Di Capua *et al.*, 2020a, 2020b), and also a process-based validation of climate models (Nowack *et al.*, 2020). However, although CENs are a useful approach to investigate causal relationships of the climate system, their application requires expertise in domain knowledge of the physical processes, careful selection of suitable time-series datasets, and sufficient sample size of the datasets (Runge, 2018).

In this study, we apply the CEN approach based on the PCMCI algorithm to analyse quantitatively the causal relationships involving the influence of ENSO on ISM precipitation over the Himalayas and the coupled interactions between MHC and RWC on intraseasonal time-scales. This is achieved by investigating the direction and strength of causal linkages between four climate indices representing ENSO, MHC, RWC, and summer monsoon Himalayan precipitation (SMHP). Following Webster *et al.* (1998), we first break down these interactions to the lowest form of complexity and then increase the complexity in steps, that is, separately testing combinations of pairs of indices in the first instance, then combinations of the indices in groups of three, and finally all four indices combined together. The remainder of this article is structured as follows. Section 2 describes the four climate indices used, as well as a description of the CEN approach based on the PCMCI algorithm and the methodology used. Section 3 presents results applying the CEN approach to examine the direction and strength of the causal linkages. In Section 4, we discuss the results obtained, both in terms of their direct causal effect (CE) and via a comparison with results using a standard correlation approach. Section 5 presents the conclusions of our study.

2 | METHODS AND MATERIALS

2.1 | Climate indices

We use monthly averaged European Centre for Medium-Range Weather Forecasts (ECMWF) Reanalysis Version 5 (ERA5) atmospheric reanalysis data (Hersbach *et al.*, 2020) to calculate monthly indices representing SMHP, MHC, and RWC for an extended summer monsoon season from May to September, which covers an 83-year period from 1940 to 2022, that is, a total of 415 months. ERA5 data combine observations and short-range weather forecasts to produce a complete and consistent estimate of

the recent state of the atmosphere from 1940 to the present day and have often been used to study precipitation over the Himalayas (e.g., Palazzi *et al.*, 2013, 2015; Wang *et al.*, 2019; Chen *et al.*, 2021; Dahri *et al.*, 2021; Kumar *et al.*, 2021; Nischal *et al.*, 2022). Using ERA5 data, (i) the SMHP index is calculated following Palazzi *et al.* (2013) as the precipitation averaged over a domain spanning 78–93°E, 25–32°N that includes much of the Himalayas (shown by the red box in Figure 1), (ii) the RWC index is calculated following Roy and Tedeschi (2016) as the (local) zonal wind at 200 hPa averaged over the same Himalayan domain used for the SMHP index, and (iii) the MHC index is calculated following Wang and Fan (1999) and Goswami *et al.* (1999) as the meridional wind shear between 850 and 200 hPa averaged over a domain spanning 70–110°E, 10–30°N that encompasses the extended monsoon region (shown by the magenta box in Figure 1). As positive RWC and MHC indices indicate a weakening of the RWC and a strengthening of the MHC, respectively, the RWC index is multiplied further by −1 in order for both indices to exhibit the same sign in response to their circulation being either strengthened or weakened. For the ENSO index, as an observation-based index is already available, we prefer to use this rather than calculate it ourselves from ERA5 data, especially as they are likely to be similar (Zhu *et al.*, 2024). We therefore use an existing ENSO index based on a five-month running mean of observed average sea-surface temperatures over the Niño 3.4 region of the tropical Pacific Ocean (i.e., 5°N–5°S, 170–120°W) to define El Niño and La Niña events (Trenberth & Stepaniak, 2001), which is calculated by the National Oceanic and Atmospheric Administration. Thus, our ENSO index is actually a combination of intraseasonal and interseasonal time-scales. A log-based transformation is applied to the SMHP index. All four indices are transformed further into detrended (monthly) anomalies to ensure that the time series are stationary, which is a requirement of the PCMCI algorithm (see below). This is achieved by removing both the seasonal and climatological cycles computed for the entire period from 1940 to 2022. Following this, the indices are standardised, which allows us to interpret the path coefficients calculated by the PCMCI algorithm (see below) as standardised effect sizes. This ensures that all variables contribute comparably and test statistics are scale-invariant, and improves numerical stability. For the extended summer monsoon period, positive SMHP, RWC, MHC, and ENSO indices therefore indicate anomalously high Himalayan precipitation, strengthening of the RWC, strengthening of the MHC, and anomalously high sea-surface temperatures in the Niño 3.4 region (i.e., analogous to the El Niño phase of ENSO), respectively.

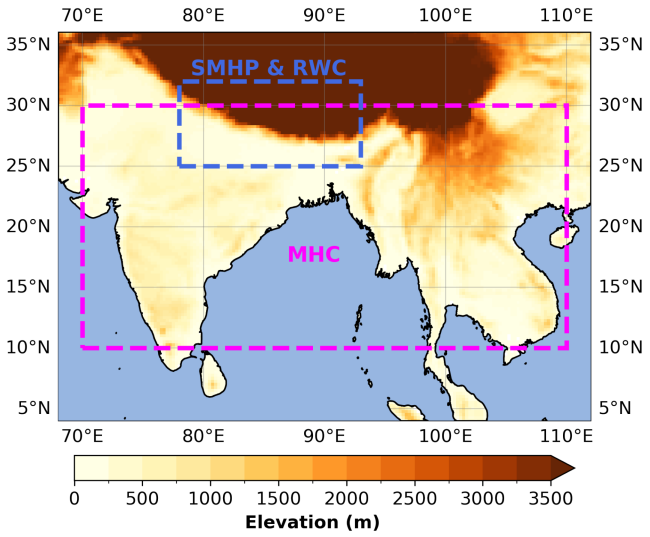

FIGURE 1 Map showing a domain spanning 78–93°E, 25–32°N that encompasses much of the Himalayas (represented by the dashed blue box), which is used for calculating the summer monsoon Himalayan precipitation (SMHP) index and the regional Walker circulation (RWC) index, as well as a domain spanning 70–110°E, 10–30°N that encompasses the extended monsoon region (represented by the dashed magenta box), which is used for calculating the monsoon Hadley circulation (MHC) index. Also shown is the orography elevation from ERA5 (shading, m).

2.2 | Causal-effect networks (CENs)

The construction of CENs is based on the PCMCI algorithm applied to a set $\boldsymbol{P}$ of time series (actors), which are detrended anomalies (Runge, 2018; Runge *et al.*, 2014; Runge *et al.*, 2019). Applying the PCMCI algorithm and the interpretation of the existence of causal links relies on assuming that the time series data are stationary and the relationships between a given set of actors are either linear or near-linear (Spirtes *et al.*, 2001). Further assumptions necessary for the PCMCI algorithm include causal sufficiency, the causal Markov condition, and faithfulness (Runge, 2018). There are two steps in the PCMCI algorithm, comprising an initial PC-step followed by the MCI-step.

The PC-step identifies the drivers (i.e., the causal parents) of each actor in $\boldsymbol{P}$ by testing all pairs of actors iteratively for conditional independence at a certain temporal lag (delay) τ. This is based on calculating partial correlations (i.e., under the assumption of linear or near-linear interactions between actors), which requires that the associated two-sided p-value from a Student's t-test meets a certain significance threshold α (Runge *et al.*, 2014, 2019). For example, if X, Y, and Z are actors in $\boldsymbol{P}$ and X and Y are conditionally dependent given Z, then this means that the correlation between X and Y cannot be (exclusively)

explained by the influence of Z. At the end of the PC-step, each actor in $\boldsymbol{P}$ has its own set of drivers or causal parents, which then enter the MCI-step.

The MCI-step again tests iteratively each possible combination of pairs of actors and the time lags for conditional independence. However, this time it uses the combined set of identified drivers of actors in the PC-step as conditioning, allowing to establish whether there is a link and whether it can be considered causal, removing spurious or common drivers and forming the final set of causal drivers for each actor (Runge *et al.*, 2014, 2019). Therefore, the subsequent procedure is a standardised multiple linear regression analysis to quantify the significance (i.e., p value) and strength of causal links. The p values obtained are corrected using the Benjamini–Hochberg false discovery rate correction (Benjamini & Hochberg, 1995; Benjamini & Yekutieli, 2001) to account for the effect of multiple testing.

The strength of the causal relationships identified is expressed as the path coefficient β of the standardised linear regression, which demonstrates how much the different causal drivers (i.e., independent variables) contribute to variability in each actor (i.e., dependent variables) in terms of standard deviations. Let us assume that the path coefficient between an actor $X^j_{t-\tau}$ (i.e., the j-th actor of the set of time series data at time $t-\tau$) and an actor X^i_t (i.e., the i-th actor of the set of time series data at time t) is defined as $\beta_{X^j_{t-\tau}\to X^i_t}$, which quantifies the expected change in X^i_t (in units of its standard deviation, SD) following an increase of $X^j_{t-\tau}$ by one SD, while keeping the other parents of X^i_t fixed (Pearl, 2013; Runge *et al.*, 2015). The sign of $\beta_{X^j_{t-\tau}\to X^i_t}$ can be explained as follows: a positive (negative) value of the path coefficient β means that an increase in $X^j_{t-\tau}$ leads to an increase (decrease) in X^i_t. Here, positive values of τ indicate that $X^j_{t-\tau}$ leads X^i_t.

The constructed CEN visualises each of the actors being examined by a node, which are connected by an arrow if the causal relationships or links between the pairs of actors are statistically significant with a p-value $< \alpha$ in the MCI-step, with the colour of the arrow representing the value of the path coefficient β of the standardised linear regression and the direction of the arrow indicating the direction of the causal link. The colour of the node corresponds to the autocorrelation path coefficient, which represents the causal influence of an actor on itself (i.e., the path coefficient $\beta_{X^j_{t-\tau}\to X^i_t}$, where $i = j$). Absolute values of the autocorrelation path coefficients are displayed to show only the strength of the coefficients (i.e., in the range from 0 to +1), as the sign is not considered, that is, based on domain knowledge, we consider the signs of the autocorrelation path coefficients as secondary information due to the short intraseasonal time-scales that are examined. If no causal link exists between an actor and itself, then a dash symbol (–) is shown instead. The associated time lags for causal links are displayed over the arrows. More details of CENs and the PCMCI algorithm can be found in Kretschmer *et al.* (2016), Runge *et al.* (2019), and Di Capua *et al.* (2020a).

2.3 | Methodology

Figure 2 presents a schematic diagram illustrating the causal relationships that we test involving the ENSO, SMHP, RWC, and MHC indices using the PCMCI algorithm to construct CENs to estimate the sign and magnitude of the path coefficients β, with a significance threshold of $\alpha = 0.05$. The causal relationships between indices are examined for a one-month time lag only, as our aim is to explore cause–effect interactions at intraseasonal time-scales. Note that the time-scales of each index used in the causal analysis are restricted to the extended summer monsoon season, that is, each year from 1940 to 2022 consists of five months of the season. Therefore, the lag of one month is sufficient to capture the lagged relationships of each monsoon season and largely prevents information from the previous year from interfering with the following one. Limiting our analysis to one-month lag, as well as the choice of a monthly time series, an extended monsoon season, and an 83-year period, was a deliberate choice to maximise the length of the indices used by the PCMCI algorithm, as this works best for a large sample size (Runge, 2018).

We first apply the CEN approach to six pairs of indices to find causal links: ENSO → RWC, ENSO → MHC, ENSO → SMHP, RWC ⇄ MHC, RWC ⇄ SMHP, and MHC ⇄ SMHP. The notation → refers to one-way interactions (i.e., direct links expressed as "from … to …") and ⇄ to two-way interactions (i.e., coupled links

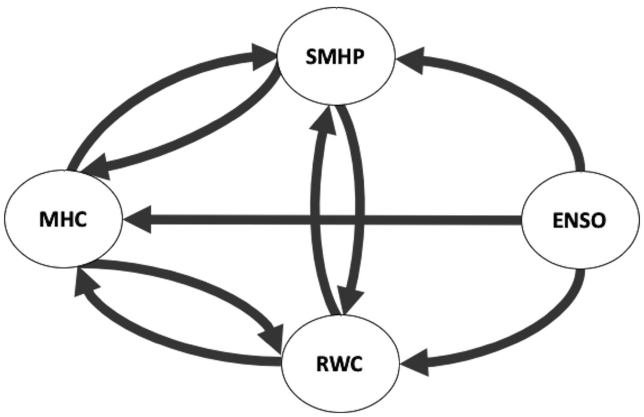

FIGURE 2 Schematic diagram illustrating the causal relationships that we test involving ENSO, SMHP, RWC, and MHC indices. A single arrow refers to one-way interactions, while two arrows refers to two-way interactions.

expressed as "between … and … ") tested by the PCMCI algorithm. For example, ENSO → RWC therefore refers to direct links from ENSO to RWC, and RWC ⇄ MHC to coupled links between RWC and MHC. Note that in our analysis any interaction with ENSO is therefore hypothesised to be one-way based on domain knowledge, which was also confirmed by the PCMCI algorithm, as it was unable to identify statistically significant links from RWC, MHC, and SMHP to ENSO (i.e., consistent with ENSO being the dominant mode of tropospheric variability in the Tropics). Following this, we increase the complexity of the CEN analysis by examining four combinations of the indices in groups of three: ENSO → RWC ⇄ MHC, ENSO → RWC ⇄ SMHP, ENSO → MHC ⇄ SMHP, and RWC ⇄ MHC ⇄ SMHP. For example, ENSO → RWC ⇄ MHC examines the one-way interaction from ENSO to both RWC and MHC, in combination with the two-way interaction between RWC and MHC. Finally, the interactions between all four indices are examined together as a single group of four, which is ENSO → RWC ⇄ MHC ⇄ SMHP. This examines the one-way interaction from ENSO to RWC, MHC, and SMHP (i.e., we do not consider the opposite effects on ENSO), in combination with the various two-way interactions between RWC, MHC, and SMHP (Webster *et al.*, 1998). Applying the CEN approach to groups of two, three, and four indices allows us to investigate the extent to which the sign and strength of path coefficients depends on the number of actors and detected linkages. For example, a link between two actors may not be apparent when they are examined as a pair, but becomes apparent when additional actors are included, that is, the causal links detected are sensitive to the chosen set or number of actors (Runge, 2018; Runge *et al.*, 2014). Additionally, as we only consider causal relationships between indices for a lag of one month, the path coefficient β represents the direct CE of the link when interactions are assumed to be linear in the causal model (Pearl, 2013; Runge, 2018; Runge *et al.*, 2023).

To assess further the statistical robustness of causal links in the constructed CENs, we apply a form of bootstrapping to the four indices examined together as a single group of four, called jackknife resampling (i.e., the resampling with replacement). This resampling procedure systematically leaves out samples corresponding to one year from each of four actors (i.e., monthly values from May to September). For each realisation of the bootstrapping, the PCMCI computes associated path coefficients. Here, we compute 400 bootstrap realisations, which is sufficiently large enough compared with the sample size. The path coefficients from each realisation are then aggregated together (i.e., the averages are calculated) to investigate their measure of spread (Δ), skewness, and sign. These realisations are also used to compute the average CE and average causal susceptibility (Runge *et al.*, 2015). The average CE measures the strength of the causal link of an actor in a given CEN on the whole network. The average causal susceptibility quantifies how strong an actor is affected by perturbations entering elsewhere in a given CEN.

3 | RESULTS

Figure 3 shows the CENs for the three pairs of indices that involve a one-way interaction with ENSO (i.e., ENSO → RWC, ENSO → MHC, and ENSO → SMHP). These results show a negative causal link for ENSO → RWC of strength $\beta_{\text{ENSO}\to\text{RWC}} = -0.20$ (Figure 3a), a negative causal link for ENSO → SMHP of strength $\beta_{\text{ENSO}\to\text{SMHP}} = -0.44$ (Figure 3b), and a negative causal link for ENSO → MHC of strength $\beta_{\text{ENSO}\to\text{MHC}} = -0.15$ (Figure 3c), that is, meaning that an increase of one SD in ENSO leads to a decrease of −0.44 SD in SMHP with a lag of one month, as well as a weaker decrease of −0.20 SD in RWC and −0.15 SD in MHC. This CEN therefore implies that, during the extended summer monsoon season, that anomalously high sea-surface temperature in the Niño 3.4 region (analogous to the El Niño phase of ENSO) will reduce Himalayan precipitation substantially, as well as weakening both the monsoon Hadley circulation and the regional Walker circulation.

Figure 4 shows the CENs for the three pairs of indices that involve two-way interactions but do not include ENSO (i.e. RWC ⇄ MHC, RWC ⇄ SMHP, and SMHP ⇄ MHC). For RWC ⇄ MHC (Figure 4a), the results show a positive causal link for RWC → MHC of strength $\beta_{\text{RWC}\to\text{MHC}} = 0.17$ (i.e., meaning that an increase of one SD in RWC leads to an increase of 0.17 SD in MHC with a lag of one month), as well as a positive causal link for the reverse link MHC → RWC with the same strength of $\beta_{\text{MHC}\to\text{RWC}} = 0.15$ (i.e., meaning that an increase of one SD in MHC leads to an increase of 0.15 SD in RWC with a lag of one month). This CEN therefore implies a positive feedback, whereby a strengthening of the regional Walker circulation results in a strengthening of the Hadley circulation, and vice versa. For RWC ⇄ SMHP (Figure 4b), the results show a positive causal link for RWC → SMHP of strength $\beta_{\text{RWC}\to\text{SMHP}} = 0.37$ at one-month lag, and a negative causal link for the reverse link SMHP → RWC with a much weaker strength of $\beta_{\text{SMHP}\to\text{RWC}} = 0.07$. This CEN therefore implies that a strengthening of the regional Walker circulation will result in a substantial enhancement of Himalayan precipitation, while any change in Himalayan precipitation has little influence on the regional Walker circulation, as illustrated by a low value of the path coefficient for this link. Finally,

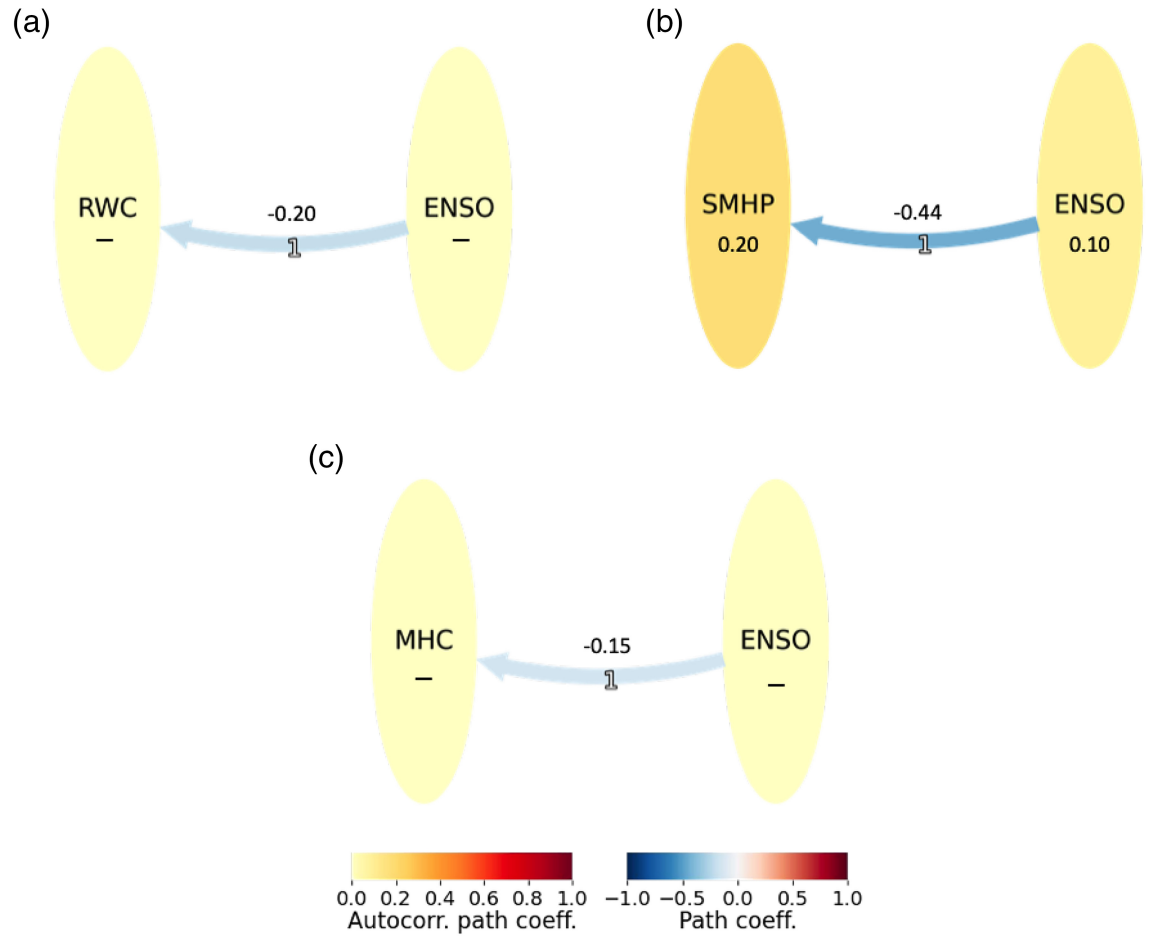

FIGURE 3 CENs showing the causal links that involve a one-way interaction with ENSO: (a) ENSO → RWC, (b) ENSO → SMHP, and (c) ENSO → MHC. For example, ENSO → RWC refers to direct links from ENSO to RWC. The nodes represent the indices, with an arrow between the nodes indicating that a statistically significant causal link has been found, with the direction of the arrow showing the direction of the link and the colour showing the path coefficient β (also shown as the value above the arrow). The colour of the nodes shows the value of the autocorrelation path coefficient, in case the index influences itself (also shown as the value shown in the node). All causal links have a time lag of one month, as our analysis is limited to this, which is shown as the value on the path coefficient β arrow.

for SMHP ⇄ MHC (Figure 4c), the results show a positive causal link for MHC → SMHP of strength $\beta_{\mathrm{MHC}\to\mathrm{SMHP}} = 0.43$ at one-month lag and a negative causal link for the reverse link SMHP → MHC with a much weaker strength of $\beta_{\mathrm{SMHP}\to\mathrm{MHC}} = -0.10$. This CEN therefore implies that a strengthening of the monsoon Hadley circulation will result in a substantial enhancement of Himalayan precipitation, albeit with the existence of a weak negative feedback, whereby enhanced Himalayan precipitation results in a slight weakening of the monsoon Hadley circulation, as illustrated by the relatively low value of the path coefficient for this link. However, it is noticeable that the strengths of the causal links/path coefficients are much larger for the links RWC → SMHP ($\beta_{\mathrm{RWC}\to\mathrm{SMHP}} = 0.37$) and MHC → SMHP ($\beta_{\mathrm{MHC}\to\mathrm{SMHP}} = 0.43$) compared with the reverse links SMHP → RWC and SMHP → MHC, that is, supporting the important influence that regional circulation fields have on Himalayan precipitation.

Figure 5 shows the CENs for the four combinations of the indices in groups of three (i.e., ENSO → RWC ⇄ SMHP, ENSO → MHC ⇄ SMHP, ENSO → MHC ⇄ RWC, and RWC ⇄ MHC ⇄ SMHP). For ENSO → RWC ⇄ SMHP (Figure 5a) and ENSO → MHC ⇄ SMHP (Figure 5b), the direction and strength of the causal links examined are similar to the results calculated when applying the CEN approach to groups of two (Figures 3 and 4). For example, for ENSO → RWC ⇄ SMHP we find the following: (i) a negative causal link for ENSO → RWC of strength $\beta_{\mathrm{ENSO}\to\mathrm{RWC}} = -0.18$ at one-month lag (compared with −0.20 in a group of two, Figure 3), (ii) a negative causal

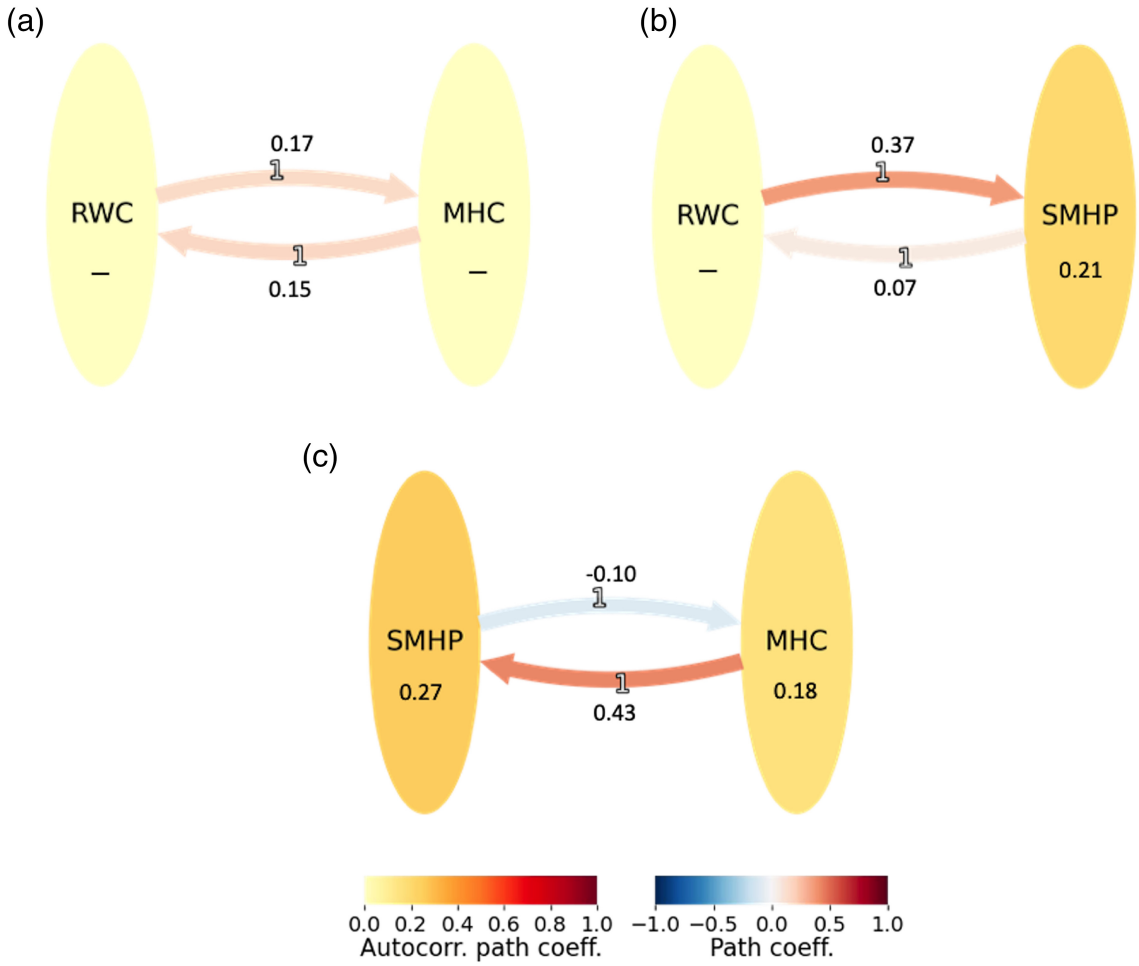

FIGURE 4 As Figure 3, but showing CENs between three pairs of indices that involve two-way interactions between (a) RWC ⇄ MHC, (b) RWC ⇄ SMHP, and (c) MHC ⇄ SMHP. For example, RWC ⇄ MHC refers to coupled links between RWC and MHC. All causal links have a time lag of one month.

link for ENSO → SMHP of strength $\beta_{\text{ENSO}\to\text{SMHP}} = -0.37$ (compared with −0.44 in a group of two, Figure 3), (iii) a positive causal link for SMHP → RWC of strength $\beta_{\text{SMHP}\to\text{RWC}} = 0.06$ (compared with 0.07 in a group of two, Figure 4), and (iv) a positive causal link for RWC → SMHP of strength $\beta_{\text{RWC}\to\text{SMHP}} = 0.34$ (compared with 0.37 in a group of two, Figure 4). For ENSO → MHC ⇄ RWC (Figure 5c), the results also show that the strengths of the causal links for MHC → RWC and RWC → MHC are broadly similar to those calculated when applying the CEN approach to groups of two (Figure 4). However, for ENSO → MHC ⇄ RWC the links for ENSO → RWC and ENSO → MHC are not found/not significant, but found/significant in a group of two (Figure 3). Reasons for these discrepancies in the results are given below in Section 4. For RWC ⇄ MHC ⇄ SMHP (Figure 5d), the results also show that the strengths of the causal links are broadly similar to those calculated when applying the CEN approach to groups of two (Figure 4), with the exception of the SMHP → RWC link. This link was not found/not significant in Figure 5, but found/significant in Figure 4 (albeit weak).

Finally, in Figure 6, the CEN for all four indices is examined together as a single group, ENSO → RWC ⇄ MHC ⇄ SMHP. This configuration confirms many of the causal links apparent from examining the indices in groups of two and three. The results confirm the strong causal links for RWC → SMHP and MHC → SMHP compared with the other links, that is, supporting the importance of the regional circulation fields for Himalayan precipitation. For example, the results using a single group show a positive causal link for RWC → SMHP of strength $\beta_{\text{RWC}\to\text{SMHP}} = 0.30$ at one-month lag (compared with 0.37 in a group of two and 0.34 and 0.32 in a group of three), and a positive causal link for MHC → SMHP of strength $\beta_{\text{MHC}\to\text{SMHP}} = 0.32$ (compared with 0.43 in a group of two and 0.35 and 0.39 in a group of three). The results also confirm the causal links for ENSO → RWC,

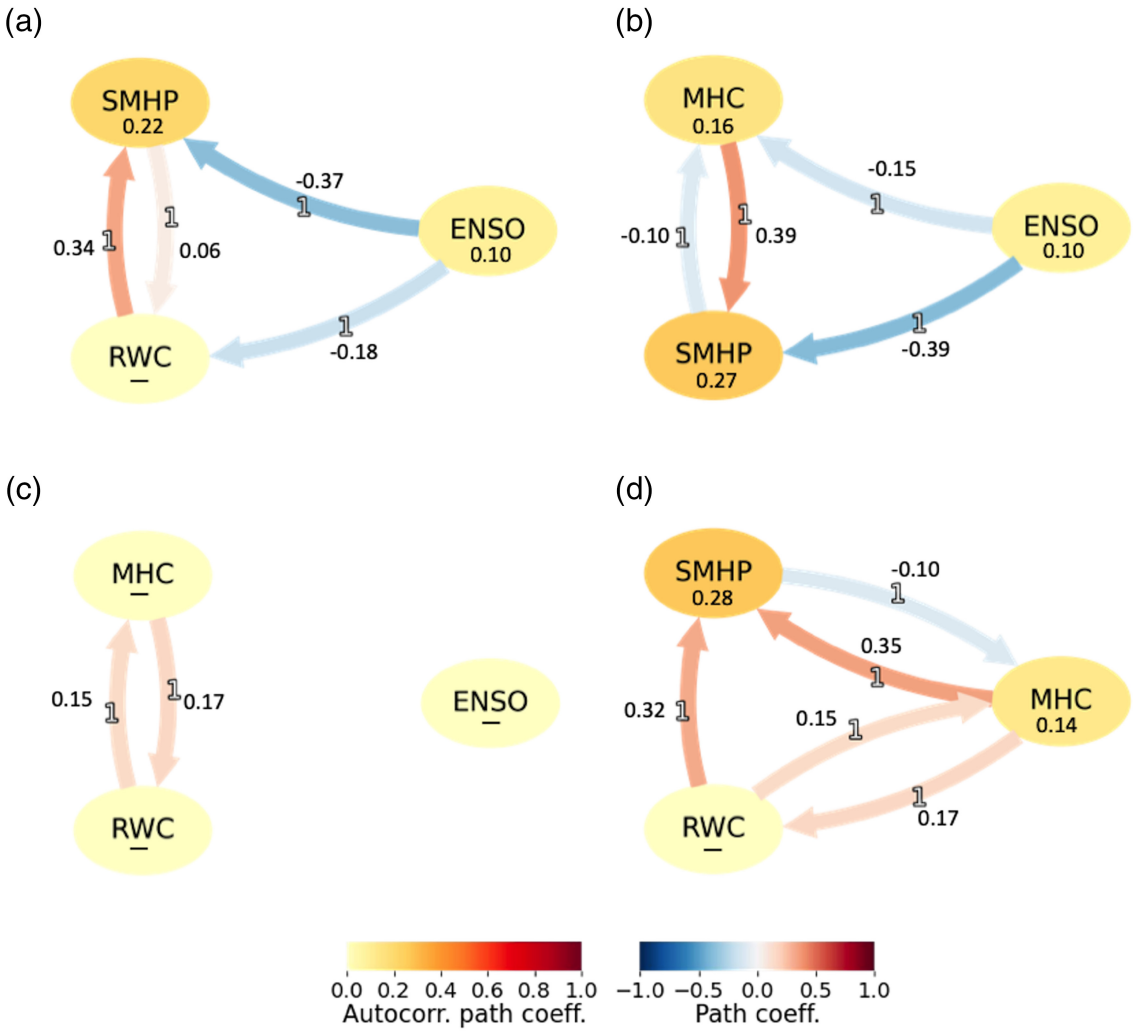

FIGURE 5 As Figure 3, but showing CENs for four combinations of the indices in groups of three: (a) ENSO → RWC ⇄ SMHP, (b) ENSO → MHC ⇄ SMHP, (c) ENSO → MHC ⇄ RWC, and (d) RWC ⇄ MHC ⇄ SMHP. Note that any interaction with ENSO is assumed to be one-way. For example, ENSO → RWC ⇄ MHC examines the one-way interaction from ENSO to RWC and MHC, in combination with the two-way interaction between RWC and MHC. All causal links have a time lag of one month.

ENSO → SMHP, and ENSO → MHC, with the strength of the ENSO → SMHP link being especially strong. For example, the results show the following: (i) a negative causal link for ENSO → SMHP of strength $\beta_{\text{ENSO}\to\text{SMHP}} = -0.33$ at one-month lag (compared with −0.44 in a group of two and −0.37 and −0.39 in a group of three), (ii) a negative causal link for ENSO → RWC of strength $\beta_{\text{ENSO}\to\text{RWC}} = -0.17$ (compared with −0.20 in a group of two and −0.18 in a group of three), and (iii) a negative causal link for ENSO → MHC of strength $\beta_{\text{ENSO}\to\text{MHC}} = -0.12$ (compared with −0.15 in a group of two and −0.15 in a group of three). Furthermore, the results using a single group confirm the positive feedback between the regional Walker circulation and the Hadley circulation, showing a positive causal link for RWC → MHC of strength $\beta_{\text{RWC}\to\text{MHC}} = 0.14$ (compared with 0.17 in a group of two and 0.15 in a group of three) and a positive causal link for MHC → RWC of strength $\beta_{\text{MHC}\to\text{RWC}} = 0.15$ (compared with 0.15 in a group of two and 0.17 in a group of three). The results also confirm a negative causal link for MHC → RWC with a relatively weak strength of $\beta_{\text{SMHP}\to\text{MHC}} = -0.10$ at one-month lag (compared with −0.10 in a group of two or three). However, the results also do not show any significant relationship for the SMHP → RWC link, which was also not apparent in a group of three and only weakly significant in a group of two ($\beta_{\text{SMHP}\to\text{RWC}} = -0.07$), that is, suggesting that the existence of this causal link is not supported.

The autocorrelation path coefficients in Figures 3–6 show the following: (i) SMHP has the strongest influence on itself among all other actors/indices, with values of 0.20,

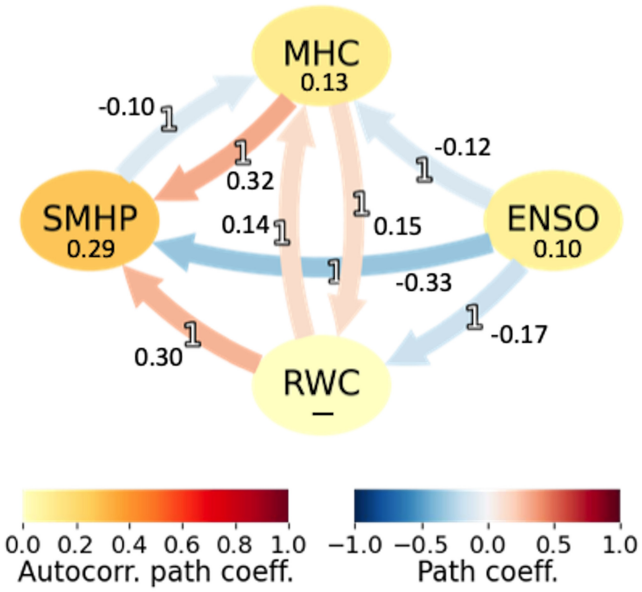

FIGURE 6 As Figure 3, but showing a CEN between all four indices examined together as a single group of four, which is ENSO → RWC ⇄ MHC ⇄ SMHP. This examines the one-way interactions from ENSO to RWC, MHC, and SMHP, in combination with the two-way interactions between RWC, MHC, and SMHP. All causal links have a time lag of one month.

0.21, and 0.27 in a group of two, 0.22 to 0.28 in a group of three, and 0.29 in a group of four, (ii) RWC is the only actor that does not have any influence on itself, (iii) ENSO has values of 0.10 or no influence at all on itself in a groups of two and three, and a value of 0.10 in a group of four, and (iv) MHC has a value of 0.18 or no influence on itself in a group of two, either 0.14 or 0.16 or no influence in a group of three, and 0.13 in a group of four. The results show that SMHP is most influenced by itself and suggest that predictions of path coefficients between SMHP and other actors may be more influenced by factors not accounted for in the causal model.

Figure 7 shows the distribution of path coefficients β computed for the established causal links using the CEN analysis with all four indices examined together as a single group, based on 400 realisations of this using the bootstrap resampling technique. The results show that the mean of the distribution for each causal link is similar to the values shown in Figure 6. The results also typically show minimum and maximum values that are relatively close to each other (and also the mean), that is, indicating a small spread (Δ) and therefore relatively robust relationships. The links with the relatively largest spread and skewness are the links ENSO → SMHP ($\Delta = 0.09$), MHC → SMHP ($\Delta = 0.09$), and MHC → RWC ($\Delta = 0.08$), whereas the link RWC → SMHP ($\Delta = 0.08$) has a relatively large range but little skewness. Importantly, the results also show that the mean, maximum, and minimum values all have the same sign, suggesting that the direction of the links is also robust.

The results from the bootstrap resampling are also used to compute mean values of the average CE and average causal susceptibility for the four indices examined together as a single group (Figure 8). The results show that the highest values of average CE are for the RWC, ENSO, and MHC (values from 0.15 to 0.20), suggesting that these have the strongest influence on the whole CEN. Moreover, MHC and RWC also have comparatively low values of the average causal susceptibility (values from 0.10 to 0.12), which suggests that they are the least vulnerable to being affected by changes from the other actors/indices. Note that the value of the average causal susceptibility for ENSO is zero, which is consistent with it having one-way feedback. By contrast, SMHP has a much lower value of the average CE (0.04) and a much larger value of the average causal susceptibility (0.31), which suggests that this has the weakest effect on the whole CEN, as well as being the most affected by changes in the other actors/indices.

4 | DISCUSSION

Although the influence of ENSO on the variability of ISM precipitation has been the focus of previous studies (e.g., Rasmusson & Carpenter, 1983; Webster & Yang, 1992; Goswami, 1994; Kumar *et al.*, 1999; Krishnamurthy & Goswami, 2000; Turner *et al.*, 2005; Mishra *et al.*, 2012; Turner & Annamalai, 2012; Wang *et al.*, 2012; Roy *et al.*, 2017; Mukherjee *et al.*, 2020), these tend to (i) be based on correlation-based metrics that do not necessarily detect cause–effect relationships, (ii) neglect how this relationship is coupled to the interaction between circulation fields representing the MHC and RWC, and (iii) focus on all-India rainfall rather than Himalayan precipitation. For this study, our aim was therefore to apply a CEN approach based on the PCMCI algorithm to analyse quantitatively the causal relationships involving the influence of ENSO on SMHP and the coupled interactions between RWC and MHC on intraseasonal time-scales. This is done by constructing causal graphs/CENs using four climate indices representing ENSO, SMHP, RWC, and MHC, and investigating the direction and strength of any causal links. Clarifying these linkages is also important for better understanding of the global-scale atmospheric circulation, as it is known that the ISM plays a crucial role in regulating the tropical meridional overturning circulation (Trenberth *et al.*, 2006).

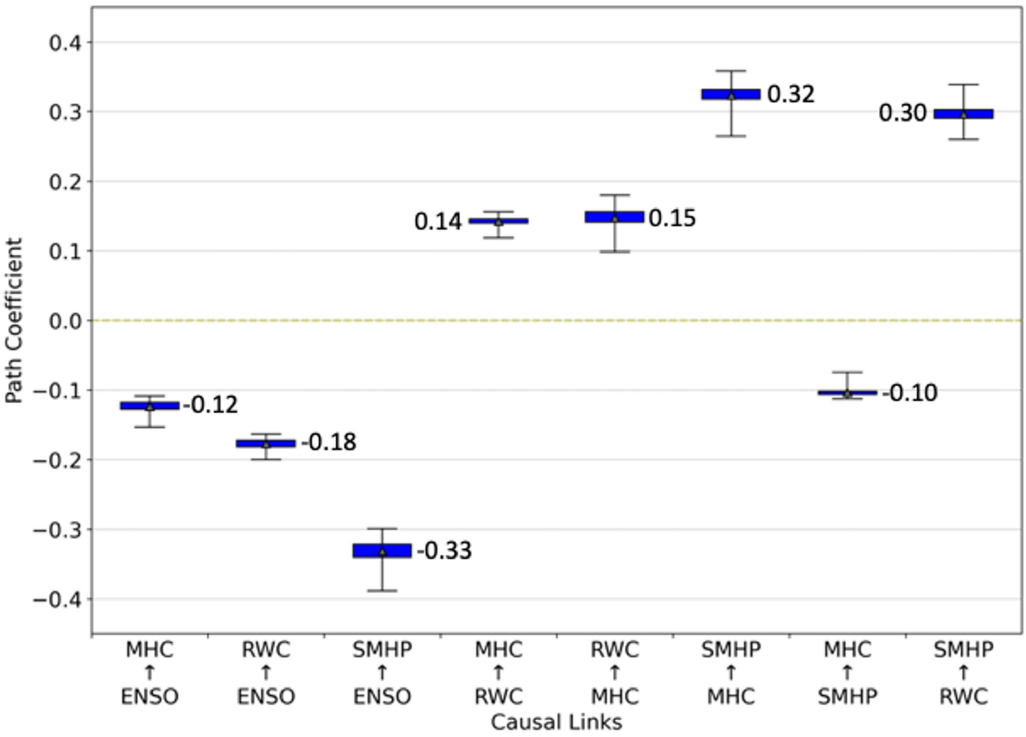

FIGURE 7 Box plots showing the distribution of the strength of the path coefficient β computed using 400 bootstrap realisations of causal links from the CEN analysis with all four indices examined together as a single group of four, which is ENSO → RWC ⇄ MHC ⇄ SMHP. This examines the one-way interaction from ENSO to either RWC or MHC or SMHP, in combination with the two-way interactions between RWC and MHC and SMHP. Note that no results are shown for SMHP → RWC, as a significant relationship for this link was not found in Figure 6. The results show the mean value (shown as the horizontal line and corresponding number), as well as the maximum and minimum values. All causal links have a time lag of one month.

The novelty of the causal analysis results is that the path coefficient β enables the strength and direction of these causal relationships to be quantified for the first time. Additionally, as we only consider relationships between indices for a lag of one month, the path coefficient β also corresponds to the direct CE. To facilitate comparison of the path coefficients/CE values based on the various CENs shown in Figures 3–6, these values are summarised in Table 1. Our results therefore tell us that the CE for the ENSO → SMHP link (depending on the complexity of the constructed CENs) has values of either −0.44 (Figure 3b), −0.37 (Figure 5a), −0.39 (Figure 5b), or −0.33 (Figure 6), that is, implying that anomalously high sea-surface temperatures in the Niño 3.4 region (analogous to the El Niño phase of ENSO) cause a substantial decrease in Himalayan precipitation, which is consistent with established understanding. Here, the strength of the CE for this link is relatively consistent, as the complexity of the constructed CENs is increased from pairs of indices (−0.44) to groups of three (−0.37 and −0.39), and finally to a single group of four (−0.33). Furthermore, the signs of the CE are consistent with the signs of an analogous correlation-based statistical analysis of these pairs of indices (Table 2), which show a negative correlation between ENSO and SMHP (correlation coefficient of −0.15). However, as stressed above, although correlation-based metrics are useful and have been used extensively to investigate the influence of ENSO on ISM precipitation (e.g., Mishra *et al.*, 2012; Bhatla *et al.*, 2016; Yang & Huang, 2021), they do not necessarily detect cause–effect relationships, and hence their interpretability is limited. Moreover, it should be noted that we focus exclusively on the direct pathways or causal effects between actors, as, by comparison, the indirect causal effects in the CENs are relatively small in magnitude. For example, for a single group of four actors, the direct causal effect from ENSO to SMHP has a value of −0.33 (Figure 6), while the indirect causal effect for ENSO → RWC → SMHP has a value of −0.05 (computed by multiplying the CE for the ENSO → RWC link by the RWC → SMHP link in Figure 6), that is, the indirect effect is an order of magnitude less than the direct effect. This also highlights that the small indirect causal effects are difficult to detect for the PCMCI algorithm because (i) these links may require more samples to be detected reliably and (ii) indirect small links might be more sensitive to strict significance levels.

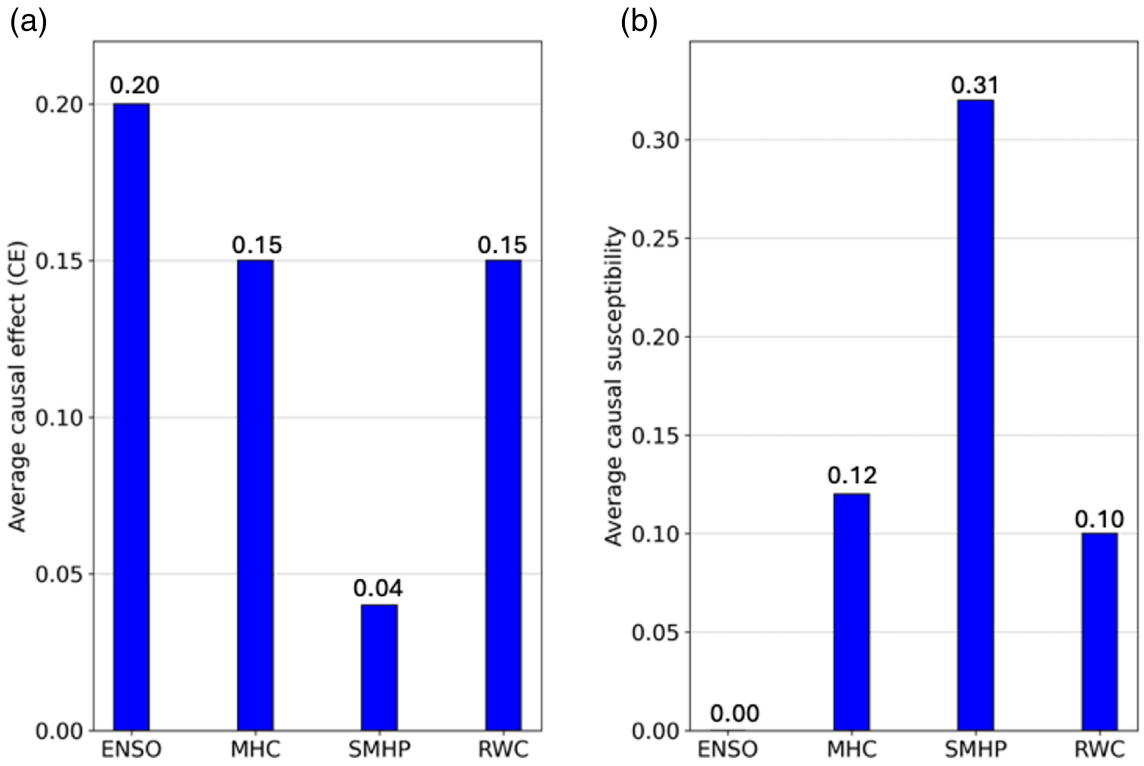

FIGURE 8 Bar charts displaying mean values of (a) the average causal effect (CE) and (b) the average causal susceptibility, computed using 400 bootstrap realisations of causal links from the CEN analysis with all four indices examined together as a single group of four, which is ENSO → RWC ⇄ MHC ⇄ SMHP. This examines the one-way interaction from ENSO to either RWC or MHC or SMHP, in combination with the two-way interactions between RWC and MHC and SMHP. All causal links have a time lag of one month.

TABLE 1 Summary of the CE values based on the path coefficients β from CENs for groups of two indices (i.e., shown in Figures 3 and 4), CENs for indices in groups of three (Figure 5), and a CEN for a single group of four indices (Figure 6). Note that for groups of three indices there are two values for the links ENSO → SMHP, MHC → SMHP, and RWC → SMHP. Additionally, for the group of four indices there is no causal link SMHP → RWC. All causal links have a time lag of one month.

	Path coefficients/CE values		
Causal link	**Groups of two indices**	**Groups of three indices**	**Groups of four indices**
ENSO → RWC	−0.20	−0.18	−0.17
ENSO → SMHP	−0.44	−0.37, −0.39	−0.33
ENSO → MHC	−0.15	−0.15	−0.12
MHC → RWC	0.15	0.17	0.15
RWC → MHC	0.17	0.15	0.14
MHC → SMHP	0.43	0.35, 0.39	0.32
SMHP → MHC	−0.10	−0.10	−0.10
RWC → SMHP	0.37	0.32, 0.34	0.30
SMHP → RWC	0.07	0.06	N/A

As well as quantifying the strength of the ENSO → SMHP teleconnection robustly, we used the causal analysis approach to clarify how this relationship is coupled to the interaction between circulation fields representing MHC and RWC. These results showed that the CE for the ENSO → RWC link has values of either −0.20 (Figure 3a), −0.18 (Figure 5a), or −0.17 SD (Figure 6), i.e, implying that an increase in ENSO causes a weakening of the regional

TABLE 2 Correlation coefficients (CCs) between the same pairs of indices shown in Figures 3 and 4 for a time lag of one month. All relationships are statistically significant (i.e., p-value < 0.05).

Pairs of indices	ENSO–SMHP	ENSO–RWC	ENSO–MHC	RWC–MHC	MHC–RWC	RWC–SMHP	SMHP–RWC	MHC–SMHP	SMHP–MHC
CCs	−0.15	−0.13	−0.12	0.19	0.14	0.19	0.11	0.10	−0.12

Walker circulation, which is consistent with established understanding. Here, the strength of the CE for this link is largely insensitive to the pairs of indices (−0.20), groups of three (−0.18), and finally a group of four (−0.17), that is, suggesting that the strength of the ENSO → RWC relationship calculated is relatively robust. However, it is noteworthy that, for the group of three involving ENSO → MHC ⇄ RWC, the ENSO → RWC link was not found/not significant (Figure 5c). For the ENSO → MHC teleconnection, the CE for this link has values of either −0.15 (Figure 3c), −0.15 (Figure 5b), or −0.12 (Figure 6), that is, implying that an increase in ENSO causes a weakening of the monsoon Hadley circulation, which is consistent with established understanding. Note that the ENSO → MHC link is slightly weaker compared with ENSO → RWC. Also, for the group of three involving ENSO → MHC ⇄ RWC, the ENSO → MHC link was also not found/not significant (Figure 5c). The signs of the CE are again consistent with the signs of an analogous correlation-based statistical analysis of these pairs of indices (Table 2), which show a negative correlation between ENSO and RWC (correlation coefficient of −0.13) and a negative correlation between ENSO and MHC (correlation coefficient of −0.12), that is, both consistent with an increase in ENSO associated with a weakening of RWC and MHC.

The causal analysis based results also show that a strengthening of both the RWC and MHC has a similarly (sizeable) impact on SMHP. For example, the CE for the MHC → SMHP link has values of either 0.43 (Figure 4c), 0.35 (Figure 5b), 0.39 (Figure 5d), or 0.32 (Figure 6), that is, implying that a strengthening of the monsoon Hadley circulation causes a substantial increase in Himalayan precipitation, which is consistent with established understanding. Here, the strength of the CE is largely insensitive to the number of actors as they are increased from two (0.43) to three (0.35 and 0.39) and finally four (0.32), that is, suggesting that the estimate of the strength of this relationship is relatively robust. The RWC → SMHP link was similar in strength and robustness to the MHC → SMHP one, with CE values of either 0.37 (Figure 4b), 0.32 (Figure 5a), 0.34 (Figure 5d), or 0.30 (Figure 6), that is, implying that a strengthening of the regional Walker circulation causes a substantial increase in Himalayan precipitation, which is consistent with established understanding. The signs of the CE are again consistent with our current understanding using correlation-based statistical analysis (Table 2), which shows a positive correlation between RWC and SMHP (correlation coefficient of 0.19) and a positive correlation between MHC and SMHP (correlation coefficient of 0.10), that is, consistent with a strengthening of either the MHC or RWC being associated with an increase in SMHP. However, the causal analysis approach again tells us that the strengths of these relationships are broadly similar, in contrast to the correlation-based analysis, which suggests a much stronger relationship between RWC and SMHP.

The causal analysis approach was also used to clarify the interaction from RWC to MHC. Using a group of two actors (Figure 4a), the CE for the RWC → MHC link was 0.17, while for the reverse MHC → RWC link it was 0.15, that is, showing a positive feedback between the monsoon Hadley circulation and the regional Walker circulation, which is consistent with established understanding. The CE for this relationship was relatively insensitive to a group of size of two (Figure 4a), three (Figure 5c), or four (Figure 6), that is, suggesting that it is relatively robust. These results complement our current understanding of these interactions over the Himalayas from the work of Roy and Tedeschi (2016) and Roy *et al.* (2017), which showed that the influence of ENSO on SMHP can be viewed as a superposition and/or interaction between the Hadley and Walker circulations over this region. Additionally, the results are also broadly consistent with our current understanding based on analogous correlation-based statistical analysis (Table 2), which shows a positive correlation between RWC and MHC (correlation coefficient of 0.19) and between MHC and RWC (correlation coefficient of 0.14).

The results also show that the MHC has a small negative feedback with precipitation, with the CE for the MHC → RWC link having values of either −0.10 (Figure 4c), −0.10 (Figure 5b), −0.10 (Figure 5d), or −0.10 (Figure 6), that is, implying that enhanced monsoon Himalayan precipitation causes a slight weakening of the monsoon Hadley circulation. Here, the strength of the CE is relatively consistent, as the complexity of the constructed CENs is increased from a group of two (−0.10) to three (−0.10) and finally four (−0.10). This is also consistent with Table 2 showing a negative correlation between SMHP and MHC (correlation coefficient of −0.12). More generally, it is also consistent with increased precipitation over the Himalayas resulting in enhanced evaporation and therefore cooling of the surface, and hence

reduced ascent over this region. By contrast, the CE for the SMHP → RWC link has values of 0.07 (Figure 4b) and 0.06 (Figure 5a), based on groups of two and three. However, it is noteworthy for the group of three involving RWC ⇄ MHC ⇄ SMHP (Figure 5d) and the group of four (Figure 6) that the SMHP → RWC link was not found/not significant. This perhaps suggests that Himalayan precipitation has little impact on the strength of the regional Walker circulation, albeit the correlation-based statistical analysis (Table 2) shows a positive correlation between SMHP and RWC (correlation coefficient of 0.11), that is, an increase in SMHP is associated with a weakening of RWC. Additionally, this is consistent with SMHP having the weakest effect on ENSO, RWC, and MHC, as well as being the most affected by changes in those indices (Figure 8).

Although we do not explore all possible drivers to construct CENs, the causal discovery approach provides a deeper understanding of the links compared with the traditional correlation-based analysis. In particular, the classical approach does not provide a reliable indication of the direction of the influence and has to be used with caution (Table 2). However, we can still distinguish a few limitations to using the CEN approach. One of these is that the set of causal drivers is based on the selected indices in this study, and adding or removing additional indices of other known influences may lead to a different CEN, that is, changing the conditional independence results in changing the linkages. For example, the analysis shows a direct link for ENSO → MHC and ENSO → RWC in pairs (Figure 3) and a group of four (Figure 6), but in a group of three (i.e., ENSO → MHC ⇄ RWC) the linkages are found to be statistically insignificant (Figure 5). This shows that the results can be sensitive to the chosen set or the number of indices/actors (Runge, 2018; Runge *et al.*, 2014). In addition, we conducted a sensitivity experiment of the free parameter α of the PCMCI algorithm for the combination ENSO → MHC ⇄ RWC in Figure 5c, which involved changing the significance level of $\alpha = 0.05$ to a less strict value of $\alpha = 0.08$ (compared with $\alpha = 0.05$ in Figure 5c) and showed that both links exist in the CEN, or are statistically significant, with $\alpha = 0.08$. This highlights that CENs are a statistical representation of physical interactions and the significance levels determine which links are visible in the network—the missing links could simply be physically real but statistically insignificant due to stringent thresholds. Nevertheless, we showed that such limitations can be overcome when possible mediators or pathways are identified for such disagreement, by gradually increasing the set of possible actors based on domain knowledge of the physical system. To this end, we showed that the CEN for all four indices examined together as a single group (Figure 6) is broadly representative of the causal links calculated based on groups of two or three indices (Figures 3–5), that is, showing that this single group of four captures the general complexity of interactions between ENSO, SMHP, MHC, and RWC (Webster *et al.*, 1998). Moreover, although we use monthly averages for our indices to build CENs, the established direct linkages may actually be causal on a weekly time-scale. Also, we recognise that our results could be sensitive to length of time series, which could be responsible for some cases in which no significant causal links are found.

Furthermore, we also explored a time lag of two months. However, because the majority of the two-month lagged causal relationships in CENs were statistically insignificant, only the results with a lag of one month are presented here. We speculate that the results with the two-month time lag were insignificant because of (i) an insufficient number of sample points for conditional independence testing in the PCMCI algorithm (i.e., this study is restricted to the period from 1940 to 2022) and (ii) considerable variability during the extended summer monsoon season resulting in the causal relationships becoming nonlinear and thus identified as statistically insignificant by the PCMCI algorithm (as one of its assumptions is that interactions between actors are linear/near-linear). Additionally, the fact that a time lag of one month yields significant results, while two months yields insignificant results, may also be because atmosphere–ocean coupling is strongest on one-month time-scales (Deser & Timlin, 1997).

In this study, we applied the CEN approach to both reanalysis and observational data, but it can also be used to test climate model data to validate the underlying processes behind intraseasonal variability, which might pave the way for improved seasonal forecasts, as well as an understanding of the causal relationships behind the interannual variability. The potential of this approach offers a pathway to reducing uncertainties in climate model projections, as well as understanding differences between models and observations. Future work could also investigate whether other drivers of the summer monsoon Himalayan precipitation can be quantified using the CEN approach, such as the Atlantic Multidecadal Oscillation and the Indian Ocean Dipole (Cai *et al.*, 2013; Di Capua *et al.*, 2020a; Goswami *et al.*, 2006; Luo *et al.*, 2011; Svendsen, 2021). It could also be used to explore how interactions among various actors have changed with time—for example, during the recent period that involves a weakening of the relationship between ENSO and ISM (Kumar *et al.*, 1999, 2006)—as well as looking into the future (Aneesh & Bódai, 2024). Additionally, the approach could also be applied to understand the causal pathways for how ENSO affects all-India rainfall.

5 | CONCLUSIONS

We used a CEN approach based on the PCMCI algorithm to analyse quantitatively the direct causal links on intraseasonal time-scales associated with the influence of ENSO teleconnections on SMHP and the coupled interactions between RWC and MHC. Our approach shows the following (depending on the complexity of the constructed CENs) on intraseasonal time-scales: (i) a CE value for the ENSO → SMHP link of −0.33 to −0.44, (ii) a CE value for the ENSO → MHC link of −0.12 to −0.15, and (iii) a CE value for the ENSO → RWC link of −0.17 to −0.20. This is interpreted as an increase in ENSO (analogous to the El Niño phase) causing a substantial decrease in Himalayan precipitation, as well as a weakening of the regional circulations. Further results showed a CE value for the MHC → SMHP link of 0.32 to 0.43 and a CE value for the RWC → SMHP link of 0.30 to 0.37. This is interpreted as a strengthening of both the regional Walker circulation and the monsoon Hadley circulation causing a substantial increase in Himalayan precipitation. Furthermore, we showed a CE value for both RWC → MHC and MHC → RWC of 0.14 to 0.17. This is interpreted as a positive feedback, whereby a strengthening of the regional Walker circulation results in a strengthening of the Hadley circulation and vice versa. Finally, we showed a CE value for the MHC → RWC link of −0.10, which implies that enhanced monsoon Himalayan precipitation causes a slight weakening of the monsoon Hadley circulation. By contrast, the SMHP → RWC link was either not found/not significant or only had a small CE value of 0.07, which implies that Himalayan precipitation has little impact on the strength of the regional Walker circulation. In general, these results add to our current understanding that the influence of ENSO on summer monsoon Himalayan precipitation can be viewed as a superposition/interaction between the Hadley and Walker circulations over this region.

ACKNOWLEDGMENTS

We are grateful for the comments from two anonymous referees on an earlier version of this article, which resulted in significant improvements to it. We also thank Reik Donner (Magdeburg–Stendal University of Applied Sciences) and Luisa Aviles Podgurski (Potsdam Institute for Climate Impact Research) for providing their expert advice on applying causal-effect networks.

FUNDING INFORMATION

G. Muszynski and J. S. Hosking were funded by Wave 1 of the UKRI Strategic Priorities Fund under the EPSRC Grants (EP/T001569/1; EP/W006022/1), particularly the "Data Science for Science" theme within those grants and The Alan Turing Institute. A. Orr and H. D. Pritchard were funded by the UKRI/NERC grant The Big Thaw: gauging the past, present and future of our mountain water resources (NE/X005267/1). G. Di Capua was supported by the BMBF through the JPI Climate/JPI Oceans NextG-Climate Science ROADMAP (01LP2002B) and the HORIZON-RIA project (101081276).

CONFLICT OF INTEREST STATEMENT

The authors declare no conflict of interest.

DATA AVAILABILITY STATEMENT

The ENSO index is available at https://psl.noaa.gov/gcos_wgsp/Timeseries/Data/nino34.long.data (last access on 05.2023).

The ERA5 monthly averaged data are available at the Copernicus Climate Change Service: https://cds.climate.copernicus.eu/cdsapp#!/dataset/reanalysis-era5-pressure-levels-monthly-means?tab=doc (last access on 05.2023).

The causal time-series analysis Python package: Tigramite 5.0.: https://github.com/jakobrunge/tigramite (last access on 02.2022).

ORCID

Grzegorz Muszynski https://orcid.org/0000-0002-6541-0698
Andrew Orr https://orcid.org/0000-0001-5111-8402
Indrani Roy https://orcid.org/0000-0003-1728-7506
Giorgia Di Capua https://orcid.org/0000-0002-7302-6522
Hamish D. Pritchard https://orcid.org/0000-0003-2936-1734
J. Scott Hosking https://orcid.org/0000-0002-3646-3504

REFERENCES

Aneesh, S. & Bódai, T. (2024) Inter-model robustness of the forced change of the Enso-Indian summer monsoon teleconnection. *NPJ Climate and Atmospheric Science*, 7(1), 4.

Benjamini, Y. & Hochberg, Y. (1995) Controlling the false discovery rate: a practical and powerful approach to multiple testing. *Journal of the Royal Statistical Society: Series B (Methodological)*, 57(1), 289–300.

Benjamini, Y. & Yekutieli, D. (2001) The control of the false discovery rate in multiple testing under dependency. *Annals of Statistics*, 29, 1165–1188.

Bhatla, R., Singh, A.K., Mandal, B., Ghosh, S., Pandey, S.N. & Sarkar, A. (2016) Influence of north Atlantic oscillation on Indian summer monsoon rainfall in relation to Quasi-Binneal oscillation. *Pure and Applied Geophysics*, 173, 2959–2970.

Bjerknes, J. (1969) Atmospheric teleconnections from the equatorial pacific. *Monthly Weather Review*, 97(3), 163–172.

Bookhagen, B. & Burbank, D.W. (2010) Toward a complete Himalayan hydrological budget: spatiotemporal distribution of snowmelt and rainfall and their impact on river discharge. *Journal of Geophysical Research. Earth Surface*, 115(F3), 1–25.

Cai, W., Zheng, X.-T., Weller, E., Collins, M., Cowan, T., Lengaigne, M. et al. (2013) Projected response of the Indian Ocean dipole to greenhouse warming. *Nature Geoscience*, 6(12), 999–1007.

Chen, Y., Sharma, S., Zhou, X., Yang, K., Li, X., Niu, X. et al. (2021) Spatial performance of multiple reanalysis precipitation datasets on the southern slope of central Himalaya. *Atmospheric Research*, 250, 105365.

Choudhury, A.D. & Krishnan, R. (2011) Dynamical response of the south Asian monsoon trough to latent heating from stratiform and convective precipitation. *Journal of the Atmospheric Sciences*, 68(6), 1347–1363.

Dahri, Z.H., Ludwig, F., Moors, E., Ahmad, S., Ahmad, B., Shoaib, M. et al. (2021) Spatio-temporal evaluation of gridded precipitation products for the high-altitude Indus basin. *International Journal of Climatology*, 41(8), 4283–4306.

Deser, C. & Timlin, M.S. (1997) Atmosphere–ocean interaction on weekly timescales in the north Atlantic and pacific. *Journal of climate*, 10(3), 393–408.

Di Capua, G., Kretschmer, M., Donner, R.V., Van Den Hurk, B., Vellore, R., Krishnan, R. et al. (2020a) Tropical and mid-latitude teleconnections interacting with the Indian summer monsoon rainfall: a theory-guided causal effect network approach. *Earth System Dynamics*, 11(1), 17–34.

Di Capua, G., Runge, J., Donner, R.V., van den Hurk, B., Turner, A.G., Vellore, R. et al. (2020b) Dominant patterns of interaction between the tropics and mid-latitudes in boreal summer: causal relationships and the role of time-scales. *Weather and Climate Dynamics Discussions*, 2020, 1–28.

Findlater, J. (1970) A major low-level air current near the Indian Ocean during the northern summer. interhemispheric transport of air in the lower troposphere over the western Indian ocean. *Quarterly Journal of the Royal Meteorological Society*, 96(409), 551–554.

Galewsky, J. (2009) Rain shadow development during the growth of mountain ranges: an atmospheric dynamics perspective. *Journal of Geophysical Research. Earth Surface*, 114(F1), 1–17.

Gill, A.E. (1980) Some simple solutions for heat-induced tropical circulation. *Quarterly Journal of the Royal Meteorological Society*, 106(449), 447–462.

Gill, E.C., Rajagopalan, B. & Molnar, P. (2015) Subseasonal variations in spatial signatures of Enso on the Indian summer monsoon from 1901 to 2009. *Journal of Geophysical Research: Atmospheres*, 120(16), 8165–8185.

Goswami, B.N. (1994) Dynamical predictability of seasonal monsoon rainfall: problems and prospects. *Proceedings of the Indian National Science Academy, Part A*, 60(1), 101–120.

Goswami, B.N. (1998) Interannual variations of Indian summer monsoon in a GCM: external conditions versus internal feedbacks. *Journal of Climate*, 11(4), 501–522.

Goswami, B.N., Krishnamurthy, V. & Annmalai, H. (1999) A broad-scale circulation index for the interannual variability of the Indian summer monsoon. *Quarterly Journal of the Royal Meteorological Society*, 125(554), 611–633.

Goswami, B.N., Madhusoodanan, M.S., Neema, C.P. & Sengupta, D. (2006) A physical mechanism for north Atlantic SST influence on the Indian summer monsoon. *Geophysical Research Letters*, 33(2), 1–4.

Gushchina, D., Zheleznova, I., Osipov, A. & Olchev, A. (2020) Effect of various types of Enso events on moisture conditions in the humid and subhumid tropics. *Atmosphere*, 11(12), 1354.

Hersbach, H., Bell, B., Berrisford, P., Hirahara, S., Horányi, A., Muñoz-Sabater, J. et al. (2020) The era5 global reanalysis. *Quarterly Journal of the Royal Meteorological Society*, 146(730), 1999–2049.

Immerzeel, W.W., Van Beek, L.P.H. & Bierkens, M.F.P. (2010) Climate change will affect the Asian water towers. *Science*, 328(5984), 1382–1385.

Kohyama, T., Suematsu, T., Miura, H. & Takasuka, D. (2021) A wall-like sharp downward branch of the walker circulation above the western Indian Ocean. *Journal of Geophysical Research. Atmospheres*, 126(21), e2021JD034650.

Kretschmer, M., Coumou, D., Donges, J.F. & Runge, J. (2016) Using causal effect networks to analyze different arctic drivers of mid-latitude winter circulation. *Journal of climate*, 29(11), 4069–4081.

Kretschmer, M., Runge, J. & Coumou, D. (2017) Early prediction of extreme stratospheric polar vortex states based on causal precursors. *Geophysical research letters*, 44(16), 8592–8600.

Krishnamurthy, V. & Goswami, B.N. (2000) Indian monsoon–Enso relationship on interdecadal timescale. *Journal of Climate*, 13(3), 579–595.

Kumar, K.K., Rajagopalan, B. & Cane, M.A. (1999) On the weakening relationship between the Indian monsoon and Enso. *Science*, 284(5423), 2156–2159.

Kumar, K.K., Rajagopalan, B., Hoerling, M., Bates, G. & Cane, M. (2006) Unraveling the mystery of Indian monsoon failure during el Niño. *Science*, 314(5796), 115–119.

Kumar, M., Hodnebrog, Ø., Daloz, A.S., Sen, S., Badiger, S. & Krishnaswamy, J. (2021) Measuring precipitation in eastern Himalaya: ground validation of eleven satellite, model and gauge interpolated gridded products. *Journal of Hydrology*, 599, 126252.

Lau, K.M. & Yang, S. (2003) Walker circulation. In: *Encyclopedia of atmospheric sciences*, Vol. 2505, 00450–4. New York: Academic Press.

Li, C. & Yanai, M. (1996) The onset and interannual variability of the asian summer monsoon in relation to land–sea thermal contrast. *Journal of Climate*, 9(2), 358–375.

Luo, F., Li, S. & Furevik, T. (2011) The connection between the Atlantic multidecadal oscillation and the Indian summer monsoon in Bergen climate model version 2.0. *Journal of Geophysical Research: Atmospheres*, 116(D19), D19117.

Lutz, A.F., Immerzeel, W.W., Shrestha, A.B. & Bierkens, M.F.P. (2014) Consistent increase in high Asia's runoff due to increasing glacier melt and precipitation. *Nature Climate Change*, 4(7), 587–592.

McGraw, M.C. & Barnes, E.A. (2018) Memory matters: a case for granger causality in climate variability studies. *Journal of Climate*, 31(8), 3289–3300.

Mishra, V., Smoliak, B.V., Lettenmaier, D.P. & Wallace, J.M. (2012) A prominent pattern of year-to-year variability in Indian summer monsoon rainfall. *Proceedings of the National Academy of Sciences of the United States of America*, 109(19), 7213–7217.

Mukherjee, S., Gosavi, V., Joshi, R. & Kumar, K. (2020) Impact of Nino phases on the summer monsoon of northwestern and eastern Himalaya. *Himalayan Weather and Climate and Their Impact on the Environment*, 19–31.

Mukherji, A., Sinisalo, A., Nüsser, M., Garrard, R. & Eriksson, M. (2019) Contributions of the cryosphere to mountain communities in the Hindu Kush Himalaya: a review. *Regional Environmental Change*, 19, 1311–1326.

Nigam, S. (1994) On the dynamical basis for the Asian summer monsoon rainfall-el Niño relationship. *Journal of Climate*, 7(11), 1750–1771.

Nischal, Attada, R. & Hunt, K.M.R. (2022) Evaluating winter precipitation over the western Himalayas in a high-resolution Indian regional reanalysis using multisource climate datasets. *Journal of Applied Meteorology and Climatology*, 61(11), 1613–1633.

Nowack, P., Runge, J., Eyring, V. & Haigh, J.D. (2020) Causal networks for climate model evaluation and constrained projections. *Nature Communications*, 11(1), 1415.

Orr, A., Ahmad, B., Alam, U., Appadurai, A.N., Bharucha, Z.P., Biemans, H. et al. (2022) Knowledge priorities on climate change and water in the upper Indus basin: a horizon scanning exercise to identify the top 100 research questions in social and natural sciences. *Earth's Future*, 10(4), e2021EF002619.

Orr, A., Listowski, C., Couttet, M., Collier, E., Immerzeel, W., Deb, P. et al. (2017) Sensitivity of simulated summer monsoonal precipitation in Langtang valley, Himalaya, to cloud microphysics schemes in WRF. *Journal of Geophysical Research: Atmospheres*, 122(12), 6298–6318.

Palazzi, E., Von Hardenberg, J. & Provenzale, A. (2013) Precipitation in the Hindu-Kush Karakoram Himalaya: observations and future scenarios. *Journal of Geophysical Research. Atmospheres*, 118(1), 85–100.

Palazzi, E., von Hardenberg, J., Terzago, S. & Provenzale, A. (2015) Precipitation in the Karakoram-Himalaya: a cmip5 view. *Climate Dynamics*, 45, 21–45.

Pearl, J. (2013) Linear models: a useful microscope for causal analysis. *Journal of Causal Inference*, 1(1), 155–170.

Rao, Y.P. (1976) *Southwest monsoon (meteorological monograph)*. New Delhi: India Meteorological Department.

Rasmusson, E.M. & Carpenter, T.H. (1983) The relationship between eastern equatorial pacific sea surface temperatures and rainfall over India and Sri Lanka. *Monthly Weather Review*, 111(3), 517–528.

Roy, I. (2018) Addressing on abrupt global warming, warming trend slowdown and related features in recent decades. *Frontiers in Earth Science*, 6, 136.

Roy, I., Tedeschi, R.G. & Collins, M. (2017) Enso teleconnections to the Indian summer monsoon in observations and models.

Roy, I. & Tedeschi, R.G. (2016) Influence of Enso on regional Indian summer monsoon precipitation-local atmospheric influences or remote influence from pacific. *Atmosphere*, 7(2), 25.

Runge, J. (2018) Causal network reconstruction from time series: from theoretical assumptions to practical estimation. *Chaos: Chaos: An Interdisciplinary Journal of Nonlinear Science*, 28(7).

Runge, J., Gerhardus, A., Varando, G., Eyring, V. & Camps-Valls, G. (2023) Causal inference for time series. *Nature Reviews Earth & Environment*, 4(7), 487–505.

Runge, J., Nowack, P., Kretschmer, M., Flaxman, S. & Sejdinovic, D. (2019) Detecting and quantifying causal associations in large nonlinear time series datasets. *Science Advances*, 5(11), eaau4996.

Runge, J., Petoukhov, V., Donges, J.F., Hlinka, J., Jajcay, N., Vejmelka, M. et al. (2015) Identifying causal gateways and mediators in complex spatio-temporal systems. *Nature Communications*, 6(1), 8502.

Runge, J., Petoukhov, V. & Kurths, J. (2014) Quantifying the strength and delay of climatic interactions: the ambiguities of cross correlation and a novel measure based on graphical models. *Journal of Climate*, 27(2), 720–739.

Sikka, D.R. (1980) Some aspects of the large scale fluctuations of summer monsoon rainfall over India in relation to fluctuations in the planetary and regional scale circulation parameters. *Proceedings of the Indian Academy of Sciences - Earth and Planetary Sciences*, 89, 179–195.

Spirtes, P., Glymour, C. & Scheines, R. (2001) *Causation, prediction, and search*. Cambridge, MA: MIT press.

Svendsen, L. (2021) The Atlantic multidecadal oscillation and Indian summer monsoon variability: a revisit. In: *Indian Summer Monsoon Variability*. Amsterdam: Elsevier, pp. 353–374.

Trenberth, K.E., Hurrell, J.W. & Stepaniak, D.P. (2006) The Asian monsoon: global perspectives.

Trenberth, K.E. & Stepaniak, D.P. (2001) Indices of el Niño evolution. *Journal of climate*, 14(8), 1697–1701.

Turner, A.G., Inness, P.M. & Slingo, J.M. (2005) The role of the basic state in the Enso–monsoon relationship and implications for predictability. *Quarterly Journal of the Royal Meteorological Society: A Journal of the Atmospheric Sciences, Applied Meteorology and Physical Oceanography*, 131(607), 781–804.

Turner, A.G. & Annamalai, H. (2012) Climate change and the south Asian summer monsoon. *Nature Climate Change*, 2(8), 587–595.

Wang, B. & Fan, Z. (1999) Choice of south Asian summer monsoon indices. *Bulletin of the American Meteorological Society*, 80(4), 629–638.

Wang, H., Wang, B., Huang, F., Ding, Q. & Lee, J.-Y. (2012) Interdecadal change of the boreal summer circumglobal teleconnection (1958–2010). *Geophysical Research Letters*, 39(12).

Wang, Y., Chen, J. & Yang, D. (2019) Bayesian assimilation of multiscale precipitation data and sparse ground gauge observations in mountainous areas. *Journal of Hydrometeorology*, 20(8), 1473–1494.

Webster, P.J., Magaña, V.O., Palmer, T.N., Shukla, J., Tomas, R.A., Yanai, M.U. et al. (1998) Monsoons: processes, predictability, and the prospects for prediction. *Journal of Geophysical Research. Oceans*, 103(C7), 14451–14510.

Webster, P.J. & Yang, S. (1992) Monsoon and Enso: selectively interactive systems. *Quarterly Journal of the Royal Meteorological Society*, 118(507), 877–926.

Wester, P., Mishra, A., Mukherji, A. & Shrestha, A.B. (2019) *The Hindu Kush Himalaya assessment: mountains, climate change, sustainability and people*. Cham: Springer Nature.

Yanai, M. & Wu, G.-X. (2006) Effects of the Tibetan Plateau.

Yang, X. & Huang, P. (2021) Restored relationship between Enso and Indian summer monsoon rainfall around 1999/2000. *The Innovation*, 2(2), 100102.

Zhu, J., Wang, W., Kumar, A., Liu, Y. & DeWitt, D. (2024) Assessment of a new global ocean reanalysis in Enso predictions with NOAA UFS. *Geophysical Research Letters*, 51(6), e2023GL106640.

How to cite this article: Muszynski, G., Orr, A., Roy, I., Di Capua, G., Pritchard, H.D. & Scott Hosking, J. (2026) Using a causal effect network approach to quantify the impact of ENSO teleconnections on summer monsoon precipitation over the Himalayas and key regional circulations. *Quarterly Journal of the Royal Meteorological Society*, 152:e70114. Available from: https://doi.org/10.1002/qj.70114